Flight Evaluation of a Sliding Mode Online Control Allocation Scheme for Fault Tolerant Control

L. Chen[1], C. Edwards[2], H. Alwi[2], M. Sato[3]

***Abstract*—This paper develops a sliding mode fault tolerant control scheme based on a Linear Parameter Varying (LPV) system representation of the plant. The scheme includes a control allocation component, which is capable of utilizing the available healthy actuators in the face of actuator faults/failures, in an effort to retain close to nominal fault free performance. The proposed scheme is validated using the Japan Aerospace Exploration Agency's Multi-Purpose Aviation Laboratory (MuPAL-α) research aircraft. The flight test results demonstrate good lateral-directional state tracking performance with no visible performance degradation in the presence of rudder and aileron faults.**

Keyword: sliding mode control, control allocation, fault tolerant control, flight test.

I. Introduction

Fault Detection and Diagnosis (FDD), and Fault Tolerant Control (FTC) have been the focus of significant attention in recent decades [1]. One of the key stakeholders in these endeavors has been the aerospace industry, because it has been noted that a significant proportion of the aircraft accidents which have occurred during the last two decades were as a result of loss of control caused by faults/failures in onboard actuator and sensor systems [3]. Most of the FDD research which has been conducted has focussed on analytic redundancy to obviate the need for hardware redundancy; whereas the efforts in terms of FTC have sought to reduce the dependency on emergency piloting skills in the face of faults/failures, while preventing unnecessarily early introduction of direct control law reconfigurations [8]. Many different paradigms have been considered in the literature as candidates for FTC including linear-quadratic regulator approaches [1], $\mathcal{H}_\infty$ methods [5], adaptive control [4] and model predictive control [6]. A state-of-the-art overview of many of these techniques and their areas of application is given in [2]; whilst [3] compares the application of many of these methods to an aerospace benchmark problem from the GARTEUR AG 16 project. In the open literature, perhaps unsurprisingly, most of the new FTC schemes have mainly been demonstrated (and compared) in simulations (see for example [3]). Notable exceptions are the pioneering propulsion controlled aircraft work by NASA Dryden which was implemented and flight tested on a MD-11 and a F-15 aircraft [9], and more recently the work by the University of Tokyo on adaptive control which was flight tested on the Japan Aerospace Exploration Agency's Multi-Purpose Aviation Laboratory (MuPAL-α) research aircraft [23]. A sliding mode approach [12] was selected as a promising method and was implemented and tested on the SIMONA motion simulator during the GARTEUR FM-AG16 project [3] (but did not undergo real in flight testing). More recently several FTC/FDD approaches were validated and demonstrated using Airbus' desktop simulator during RECONFIGURE. All these projects sought to narrow the (increasing) gap between the FDD/FTC approaches developed by the academic community and the practical demands from industry.

The most recent in a line of EU funded projects exploring the potential of FDD/FTC for aircraft flight control systems is the H2020/Japan co-funded project VISION. The aim of the project is to develop and validate FDD/FTC techniques for improving aircraft Guidance, Navigation and Control (GNC), whilst increasing the Technology Readiness Level (TRL) of modern FDD/FTC techniques to Tier 7. In the framework of VISION, advanced FDD/FTC approaches are being validated and evaluated at a system integration level – in part using the MuPAL-α research aircraft [10].

Sliding Mode Control (SMC) schemes [12] have attracted attention because of their inherent ability to reject so-called matched uncertainty – i.e. uncertainty occurring in the channels in which the control signals act. Actuator faults and failures, by definition, act in these channels, and therefore can be considered as a particular form of matched uncertainty. As a consequence, sliding mode controllers are a natural candidate for FTC. To widen their capabilities further, such schemes can be incorporated within a simple Control Allocation (CA) framework (for over-actuated systems) to deal with total actuator failures [16]. This scheme was selected as one of the two designs chosen for implementation and demonstration on the SIMONA flight simulator as part of the GARTEUR project [3].

In recent years, Linear Parameter Varying (LPV) based synthesis methodologies [11], [19] have been widely considered in aerospace applications to ensure robustness and stability over a wide range of flight conditions. *In this paper, a new LPV sliding mode FTC scheme is developed and implemented within MuPAL-α's experimental Fly-By-Wire (FBW) system.* The scheme combines the inherent robustness of SMC to actuator faults, together with an online CA framework and builds on the scheme from [16]. In terms of the design of

[1]School of Aerospace, Transport & Manufacturing, Cranfield University, UK
[2]College of Engineering, Mathematics & Physical Sciences, University of Exeter, UK
[3]Japan Aerospace Exploration Agency, Mitaka, Tokyo 181-0015, Japan

sliding mode control schemes for LPV systems, very little exists in terms of previous literature. The most recent relevant work is from [7], but because of the proportional tracking error structure, it does not exhibit to the state feedback structure which is considered here. The work in [13] is also related but considers a specific class of (quasi) LPV system in which the scheduling variables are the states themselves and the representation is obtained from an underlying nonlinear input-affine form. The approach proposed in this paper is applicable to a wide class of LPV systems and allows the input distribution matrix to be scheduling parameter-dependent. Furthermore, in contrast to [7], the focus here is on FTC. The paper focusses on lateral-directional control, and fault scenarios in which the ailerons and the rudder work at reduced levels of effectiveness. This scheme is shown to have the capability to cope with total actuator failures using differential thrust as a further level of redundancy, where the objective is to retain as close to nominal fault free performance despite actuator faults/failures. The main contribution of the paper is that it describes the *first* implementation, evaluation and validation of a sliding mode CA scheme on a real full scale aircraft involving piloted flight tests.

II. LPV SLIDING MODE CONTROLLER DESIGN

In this section, a sliding mode FTC scheme with online CA is developed from a theoretical standpoint based on an LPV model of the system. Consider the system

$$\begin{aligned} \dot{x}_p(t) &= A_p(\rho)x_p(t) + B_p(\rho)(I_m - K(t))u(t) + D_p(\rho)\xi(t) \\ y(t) &= C_p(\rho)x_p(t) \end{aligned} \tag{1}$$

where $A_p(\rho) \in \mathbb{R}^{n\times n}$, $B_p(\rho) \in \mathbb{R}^{n\times m}$ and $C_p(\rho) \in \mathbb{R}^{l\times n}$. The plant states and the control inputs are respectively denoted by $x_p \in \mathbb{R}^n$ and $u \in \mathbb{R}^m$ whilst $y(t) \in \mathbb{R}^l$ where, $l < m$, is the controlled output. This redundancy will be exploited to achieve fault tolerant control even in the case of a class of total failures. The disturbance distribution matrix $D_p(\rho) \in \mathbb{R}^{n\times k}$, and the unknown but bounded signal $\xi(t) \in \mathbb{R}^k$ denotes a 'matched' disturbance (see Assumption 2.2). The scheduling parameter $\rho \in \mathbb{R}^{n_r}$ is assumed to be differentiable and lies in a hyper-rectangle $\Omega \subset \mathbb{R}^{n_r}$ with $N = 2^r$ vertices. In system (1), the diagonal matrix $K(t) := \mathrm{diag}(k_1(t), \ldots, k_m(t))$ where the time varying scalars $k_1(t), k_2(t), \ldots k_m(t)$ model the loss of effectiveness of the actuators [12]. This is a specific form of one of the fault models used extensively in the literature. A fault-free actuator is modelled as $k_j(t) = 0$ and for a completely failed actuator $k_j(t) = 1$. When $0 < k_j(t) < 1$, the actuator behaves with reduced effectiveness (i.e. it is faulty but has not failed). The following assumptions are used throughout the paper.

Assumption 2.1: Assume the system matrices $A_p(\rho)$ and $C_p(\rho)$ in (1) are affinely dependent on ρ (this assumption can be relaxed for matrices $B_p(\rho)$ and $D_p(\rho)$), in particular

$$A_p(\rho) = A_{p,0} + A_{p,1}\rho_1(t) \ldots + A_{p,n_r}\rho_{n_r}(t) \tag{2}$$

Assumption 2.2: The uncertainty in (1) is matched: specifically the range spaces $\mathcal{R}(D_p(\rho)) \subseteq \mathcal{R}(B_p(\rho))$ for all $\rho \in \Omega$. Furthermore it is assumed $\|\xi(t)\| \leq \alpha(t, x)$ for some known positive bounded scalar function $\alpha(t, x)$.

Define the effectiveness matrix $W(t) \in \mathbb{R}^{m\times m}$ as

$$W(t) := I_m - K(t) \tag{3}$$

and as a consequence, the ith diagonal element of $W(t)$ is $w_i(t) = 1 - k_i(t)$ and $w_i(t) \in [0, \ \ 1]$. To simplify the design process, assume:

Assumption 2.3: Assume the input distribution matrix can be factorized as

$$B_p(\rho) = B_v B_2(\rho) \tag{4}$$

where $B_v \in \mathbb{R}^{n\times l}$ is a fixed matrix with full column rank, and the time varying matrix $B_2(\rho) \in \mathbb{R}^{l\times m}$. Furthermore, assume $\mathrm{rank}(B_2(\rho)) = l < m$ for all $\rho \in \Omega$.

Variations on this form of factorization are common in the FTC literature when considering control allocation and systems with redundancy (see for example [12], [17]).

Since by assumption $\mathrm{rank}(B_v) = l$ there exists a coordinate change of the form $x_p \mapsto T_n x_p = x$ such that

$$T_n B_v = \begin{bmatrix} 0 & I_l \end{bmatrix}^T \tag{5}$$

In the literature this decomposition of the input distribution matrix results in so-called regular form [18]. In the new coordinate system, (1) can be written as

$$\dot{x}(t) = A(\rho)x(t) + \begin{bmatrix} 0 \\ B_2(\rho) \end{bmatrix} W(t)u(t) + \begin{bmatrix} 0 \\ D_2(\rho) \end{bmatrix} \xi(t) \tag{6}$$

where $A(\rho) = T_n A_p(\rho) T_n^{-1}$ and $D_2(\rho) \in \mathbb{R}^{l\times k}$. This special structure of the uncertainty distribution matrix is due to Assumption 2.3.

Define a virtual control input $v(t) \in \mathbb{R}^l$ according to

$$v(t) := B_2(\rho)W(t)u(t) \tag{7}$$

The objective is to first design the virtual control $v(t)$ to provide appropriate closed loop performance, and then to compute the physical control law $u(t)$ so that equation (7) is satisfied. Substituting from (7) in (6) yields

$$\dot{x}(t) = A(\rho)x(t) + \begin{bmatrix} 0 \\ I_l \end{bmatrix} v(t) + \begin{bmatrix} 0 \\ D_2(\rho) \end{bmatrix} \xi(t) \tag{8}$$

The design of the virtual control $v(t)$ is based on the nominal system in (8). Here it is proposed the actual control signals sent to the physical actuators are

$$u(t) := N(\rho)v(t) \tag{9}$$

where the allocator matrix[1]

$$N(\rho) := \Lambda(t)B_2^T(\rho)(B_2(\rho)\Lambda(t)^2 B_2^T(\rho))^{-1} \tag{10}$$

and $\Lambda(t) \in \mathbb{R}^{m\times m}$ is any diagonal weighting matrix such that $\det(B_2(\rho)\Lambda(t)^2 B_2^T(\rho)) \neq 0$. *Here, it is assumed* $\Lambda(t)$ *is a diagonal matrix representing an online estimate of the effectiveness matrix* $W(t)$. The $\Lambda(t)$ is assumed to be computed by the monitoring scheme to approximate, as accurately

[1]The motivation for $N(\rho)$ is discussed in Remark 2.1.

as possible, the effectiveness matrix $W(t)$, and its diagonal elements are assumed to satisfy

$$0 < \Lambda_{ii}(t) \leq 1 \quad \text{for} \quad i = 1 \cdots m \tag{11}$$

As a consequence, $\|\Lambda(t)\| \leq 1$. In general $\Lambda(t) \neq W(t)$, but here the following assumption is imposed.

Assumption 2.4: The weighting $\Lambda(t)$ can be written as

$$\Lambda(t) = (I + \Delta(t))^{-1} W(t) \tag{12}$$

where the diagonal matrix $\Delta(t) \in \mathbb{R}^{m \times m}$ encapsulates the imprecision in the estimate of $W(t)$ by $\Lambda(t)$.

Remark 2.1: In an ideal situation when the estimation is perfect, $\Delta(t) = 0$ and it follows from equation (12) that $\Lambda(t) = W(t)$. In this case $u(t)$ from (9) and (10) satisfies (7) since $B_2(\rho)W(t)N(\rho) = I$. (Although the general case when $\Delta \neq 0$ is considered throughout.)

For the developments which follow, define the set

$$\begin{aligned} \mathcal{W}_\varepsilon = \Big\{ &\text{Diagonal matrices } \Lambda(t) \text{ satisfying (11) s.t.} \\ &\lambda_{min}(B_2(\rho)\Lambda(t)^2 B_2^T(\rho)) > \varepsilon \text{ for all } \rho \in \Omega \Big\} \end{aligned} \tag{13}$$

where $0 < \varepsilon < 1$ is a small design scalar. Then for any $\Lambda(t) \in \mathcal{W}_\varepsilon$, $\det(B_2(\rho)\Lambda(t)^2 B_2^T(\rho)) \neq 0$, and the allocation structure $N(\rho)$ in (10) is well defined.

Remark 2.2: The larger ε, the more stringent the constraint in (13) and the smaller the allowable set $\mathcal{W}_\varepsilon$ in the sense that if two scalars satisfy $\varepsilon_1 > \varepsilon_0 > 0$ then $\mathcal{W}_{\varepsilon_1} \subset \mathcal{W}_{\varepsilon_0}$.

It follows $\|N(\rho)\|$ is bounded for all $\Lambda(t) \in \mathcal{W}_\varepsilon$ and $\rho \in \Omega$ because from its definition in (10)

$$\|N(\rho)\| \leq \|\Lambda\| \|B_2(\rho)\| \|(B_2(\rho)\Lambda^2 B_2^T(\rho))^{-1}\| < \frac{1}{\varepsilon} \|B_2(\rho)\| \tag{14}$$

To facilitate the control law design, partition the states in (8) as $x(t) = \text{col}(x_1(t), x_2(t))$ where $x_1(t) \in \mathbb{R}^{(n-l)}$ and $x_2(t) \in \mathbb{R}^l$ then (8) can be written as

$$\begin{bmatrix} \dot{x}_1 \\ \dot{x}_2 \end{bmatrix} = \begin{bmatrix} A_{11}(\rho) & A_{12}(\rho) \\ A_{21}(\rho) & A_{22}(\rho) \end{bmatrix} \begin{bmatrix} x_1 \\ x_2 \end{bmatrix} + \begin{bmatrix} 0 \\ I_l \end{bmatrix} v + \begin{bmatrix} 0 \\ D_2(\rho) \end{bmatrix} \xi \tag{15}$$

Assumption 2.5: Assume the pair $(A_{11}(\rho), A_{12}(\rho))$ is quadratically stabilizable for all $\rho \in \Omega$.

Define a parameter-dependent switching function as

$$s(t) = S(\rho)x(t) \tag{16}$$

Exploiting the regular form structure in (15), choose

$$S(\rho) := \begin{bmatrix} M(\rho) & I_l \end{bmatrix} \tag{17}$$

where $M(\rho) \in \mathbb{R}^{l \times (n-l)}$ represents the design freedom. During a sliding motion $s(t) = 0$, and therefore from (16) and (17), during sliding

$$x_2(t) = -M(\rho)x_1(t) \tag{18}$$

Substituting (18) into (15) yields

$$\dot{x}_1(t) = (A_{11}(\rho) - A_{12}(\rho)M(\rho))x_1(t) \tag{19}$$

The dynamics associated with (19) constitute the sliding motion. In the sequel, two methods will be proposed to calculate $M(\rho)$. The choice of $M(\rho)$ can be thought of as an LPV state feedback problem for the pair $(A_{11}(\rho), A_{12}(\rho))$ in (19). Here the polytopic LPV based approach is adopted as the basis for the developments (although other options in the literature could be pursued: see for example [11]).

Let $\bar{A}_{11,i}$ and $\bar{A}_{12,i}$ represent the values of $A_{11}(\rho)$ and $A_{12}(\rho)$ in terms of the ith vertex of Ω so that

$$A_{11}(\rho) = \sum_{i=1}^{N} p_i(\rho)\bar{A}_{11,i}, \;\; A_{12}(\rho) = \sum_{i=1}^{N} p_i(\rho)\bar{A}_{12,i} \tag{20}$$

and

$$M(\rho) = \sum_{j=1}^{N} p_j(\rho)\bar{M}_j \tag{21}$$

where $N = 2^{n_r}$ represents the number of vertices of Ω, $\bar{M}_j$ is the jth vertex of $M(\rho)$, and the scalars $p_i(\rho) \geq 0$ satisfy the simplex expression $\sum_{i=1}^{N} p_i(\rho) = 1$. Define

$$\Psi_{ij} = \bar{A}_{11,i}P_1 - \bar{A}_{12,i}Y_j \tag{22}$$

where P_1 is a symmetric positive definite (s.p.d) matrix and Y_j represents a matrix of appropriate dimension.

Theorem 1: If there exist a symmetric positive definite matrix P_1 and matrices Y_j such that the LMIs

$$\Psi_{ij} + \Psi_{ij}^T < 0 \tag{23}$$

are feasible for all $i, j = 1, \ldots, N$, then the system in (19), representing the sliding motion, is quadratically stable.

Proof: Similar to [19]. ■

Remark 2.3: Note: other LMI conditions to (23) to guarantee stability can be found in [14], [15].

In the sliding mode literature for LTI systems, one of the early methods for hyperplane design was based on quadratic optimal control exploiting 'cheap control' [18]. In the context of this paper, the corresponding formulation is: minimize by choice of $M(\rho)$ the cost

$$J = \int_{t_s}^{\infty} x_1^T(\tau)Q_{11}x_1(\tau) + x_1^T(\tau)M^T(\rho)Q_{22}M(\rho)x_1(\tau)d\tau \tag{24}$$

subject to the system (19) where Q_{11} and Q_{22} are s.p.d[2] and t_s is the time at which sliding occurs.

Theorem 2: Suppose there exist a s.p.d matrix P_1 and matrices Y_j such that the LMIs

$$\begin{bmatrix} \Psi_{ij} + \Psi_{ij}^T & Y_j^T Q_{22} & P_1 Q_{11} \\ * & -Q_{22} & 0 \\ * & * & -Q_{11} \end{bmatrix} < 0 \tag{25}$$

are feasible for all $i, j = 1, \ldots, N$ where the Ψ_{ij} are defined in (22). Then if the jth vertex of $M(\rho)$ is defined as $\bar{M}_j = Y_j P_1^{-1}$ for $j = 1, \ldots, N$ and $M(\rho)$ is given by (21), the system in (19) is quadratically stable and the LQR performance cost defined in (24) satisfies $J \leq x_1^T(t_s)P_1^{-1}x_1(t_s)$.

Proof: Considering $V_1(x_1) = x_1^T(t)P_1^{-1}x_1(t)$ as a Lyapunov function candidate, standard manipulations, such as those presented in [20], yield the result. ■

[2]Equation (24) is an extension of equation (4.40) in Section 4.2.2 of [18] from an LTI setting to an LPV formulation.

In this section, a virtual control law is proposed to ensure a sliding motion occurs on the time-varying surface

$$\mathcal{S} := \{x \in \mathbb{R}^n : S(\rho)x = 0\} \tag{26}$$

The virtual control is chosen to have the structure

$$v(t) = v_l(t) + v_n(t) \tag{27}$$

where the state feedback LPV gain term

$$v_l(t) = -S(\rho)A(\rho)x(t) - \dot{M}(\rho)x_1(t) + \Phi s(t) \tag{28}$$

In (28) $\Phi \in \mathbb{R}^{l\times l}$ is a user defined fixed Hurwitz matrix, whilst the term

$$v_n(t) = -\mathcal{K}(t,x)\frac{P_2 s(t)}{\|P_2 s(t)\|} \quad \text{if} \quad s(t) \neq 0 \tag{29}$$

where $\mathcal{K}(t,x)$ is a positive scalar modulation function, and since Φ is Hurwitz, P_2 is the s.p.d matrix satisfying $P_2\Phi + \Phi^T P_2 = -I_l$. This controller structure is derived from [18] and has a flexible architecture with well understood tuning functionality which is useful from a developmental point of view in terms of implementation and testing. For example, the nonlinear term $v_n(t)$ can be 'discarded' by choosing $\mathcal{K}(t,x) = 0$ to leave a linear controller.

In preparation for the main theorem in this section define

$$B_2^\dagger(\rho) = \Lambda(t)^2 B_2^T(\rho)(B_2(\rho)\Lambda(t)^2 B_2^T(\rho))^{-1} \tag{30}$$

for all $\rho \in \Omega$ and $\Lambda \in \mathcal{W}_\varepsilon$. Notice that $B_2^\dagger(\rho)$ is a right pseudo inverse of $B_2(\rho)$ since $B_2(\rho)B_2^\dagger(\rho) = I$ for all $\rho \in \Omega$ and $\Lambda \in \mathcal{W}_\varepsilon$. Furthermore using similar arguments to those used to obtain inequality (14), it can be shown for all $\rho \in \Omega$ and $\Lambda \in \mathcal{W}_\varepsilon$ that

$$\|B_2^\dagger(\rho)\| < (1/\varepsilon)\|B_2(\rho)\| \tag{31}$$

and so $\|B_2^\dagger(\rho)\|$ is bounded for all $\rho \in \Omega$. The main theorem will now be presented.

Theorem 3: Let Δ_{max} be a user defined scalar satisfying $0 < \Delta_{max} < 1$ scalar, so that the error in estimation precision $\Delta(t)$ defined in (12) satisfies

$$\|\Delta(t)\| < \frac{1-\Delta_{max}}{\|B_2(\rho)\|\|B_2^\dagger(\rho)\|} \tag{32}$$

for all $\Lambda \in \mathcal{W}_\varepsilon$ and $\rho \in \Omega$. Then if $\eta > 0$ is a small positive scalar and the modulation gain in (29) satisfies

$$\mathcal{K}(t,x) \geq \frac{\|D_2(\rho)\|\alpha(t,x) + \eta + (1-\Delta_{max})\|v_l\|}{\Delta_{max}} \tag{33}$$

a sliding motion takes place on $\mathcal{S}$ in finite time.

Proof: This is similar to the arguments in [22] and [13] and is sketched here. Simple calculations show

$$B_2(\rho)W(t)u = v(t) + B_2(\rho)\Delta(t)B_2^\dagger(\rho)v(t) \tag{34}$$

where the definitions of $N(\rho)$ and $B_2^\dagger(\rho)$ in (10) and (30) have been exploited. From (16) and (17), and using (6)-(12) and (30), the derivative of the switching function is

$$\dot{s}(t) = S(\rho)\dot{x}(t) + \dot{M}(\rho)x_1(t)$$

Then substituting (6) and (34) into the above yields

$$\dot{s} = S(\rho)A(\rho)x + B_2(\rho)\Delta B_2^\dagger(\rho)v + v + D_2(\rho)\xi + \dot{M}(\rho)x_1$$

Substituting for the control components (28) and (29)

$$\dot{s} = \Phi s - \mathcal{K}\frac{P_2 s}{\|P_2 s\|} + D_2(\rho)\xi + B_2(\rho)\Delta B_2^\dagger(\rho)v \tag{35}$$

Consider as a candidate Lyapunov function for (35) the expression $V(s) = s^T P_2 s$. Differentiating with respect to time and then exploiting (35) it can be shown that

$$\dot{V} = -\|s\|^2 - 2\mathcal{K}\|P_2 s\| + 2s^T P_2(D_2(\rho)\xi + B_2(\rho)\Delta B_2^\dagger(\rho)v) \tag{36}$$

Furthermore, it follows from (32) that

$$\|B_2(\rho)\Delta B_2^\dagger(\rho)\| < \|B_2(\rho)\|\|\Delta\|\|B_2^\dagger(\rho)\| \leq 1 - \Delta_{max}$$

and therefore from (36)

$$\begin{aligned}
\dot{V} &\leq -\|s\|^2 - 2\|P_2 s\|(\mathcal{K} - \|D_2(\rho)\|\|\xi\| - (1-\Delta_{max})\|v\|) \\
&\leq -\|s\|^2 - 2\|P_2 s\|(\mathcal{K} - \|D_2(\rho)\|\|\xi\| \\
&\qquad -(1-\Delta_{max})(\|v_l\| + \|v_n\|)) \\
&\leq -\|s\|^2 - 2\|P_2 s\|(\Delta_{max}\mathcal{K} - \|D_2(\rho)\|\|\xi\| \\
&\qquad -(1-\Delta_{max})\|v_l\|)
\end{aligned} \tag{37}$$

Substituting (33) into (37) yields

$$\dot{V}(s) \leq -\|s\|^2 - 2\eta\|P_2 s\| \leq -2\bar{\eta}\sqrt{V} \tag{38}$$

where $\bar{\eta} = \eta\sqrt{\lambda_{min}(P_2)}$. Since $\bar{\eta} > 0$, inequality (38) implies $V = 0$ in finite time and therefore $s = 0$ in finite time and sliding is attained and can be maintained for all subsequent time. ■

III. MuPAL-α and control design

The theoretical developments in Section II will be employed to create a lateral directional FTC controller for the MuPAL-α aircraft (see Fig. 1) owned by the Japan Aerospace Exploration Agency (JAXA). The MuPAL-α is a twin-propeller engine Dornier Do228-202 aircraft which has been modified to implement an experimental (research) FBW system and Direct Lift Control (DLC) flaps [10]. The FBW computer is based on a Motorolla 68040 chip giving 44 MIPS @ 40MHz. This provides rather modest computational performance compared with more modern chips. This aircraft has been used for evaluating human-machine interactions, and testing state-of-the-art control, guidance and navigation technologies [10]. New flight control strategies can be implemented and evaluated firstly on the ground (in a Hardware-in-the-loop (HIL) configuration) (see for example [21]) and then by piloted flight evaluation.

Fig. 1. MuPAL-α aircraft

During flight tests, the safety pilot can take over control at any time and override the FBW system via the original Do228's direct mechanical linkages from the pilot inputs (wheel, column, pedal and throttle levers).

Here, the scheduling parameters have been selected as $\rho = [\ v_{eas} \quad v_{eas}^2\ ]$. The second component v_{eas}^2 has been included to provide greater fidelity in terms of modelling accuracy[3] and is treated (somewhat conservatively) as being independent of v_{eas}. Both scheduling parameters have been scaled to the range $[0,\ 1]$. The controller was designed under the following conditions:

- altitude of $5000\ ft$ at standard atmosphere conditions;
- flaps and gear set to up, and the DLC flaps at $0\ deg$;
- a weight of $5700\ kg$, and c.g. at 28%.
- equivalent airspeed ranges from $100\ kts$ to $200\ kts$.

This paper will focus on lateral-directional control (largely because it affords redundancy in terms of fault tolerant control). The system states and inputs are:

$$x_p = \begin{bmatrix}\phi & \beta & r & p\end{bmatrix}^T \quad \text{and} \quad u = \begin{bmatrix}\delta_{td} & \delta_a & \delta_r\end{bmatrix}^T \tag{39}$$

where ϕ denotes roll angle (rad), β denotes sideslip angle (rad), r represents yaw rate (rad/s) and p is roll rate (rad/s), δ_{td} represents differential power lever deviation, and δ_a and δ_r represent the aileron (rad) and rudder (rad) surface deflections. The controlled outputs are the sideslip angle and the roll angle.

Under mild assumptions, as described in [17], [25], [22], the input distribution matrix can be factorized as in (4) [22]. In Assumption 2.3, the rank condition of $\|B_2(\rho)\|$ can be verified using the full rank test in [26]. Here the uncertainty $\xi(t)$ includes wind/gusts occurring in the yaw and roll rate channels. These constitute so-called matched disturbances [22], and can be rejected by the sliding mode controller. Finally Assumption 2.5 can be verified based on [27]. To create a steady state reference tracking capability, in this paper, integrator states are introduced according to

$$\dot{x}_r(t) = y_c(t) - C_p(\rho)x_p(t) \tag{40}$$

where $y_c(t)$ is the (differentiable) command signal. Here it is assumed $y_c(t)$ is a smooth low pass filtered signal arising from a piecewise constant reference [18]. Define the augmented state vector $x_a = \mathrm{col}(x_r, x_p)$ and create using (1) and (40) the augmented state space system

$$\dot{x}_a(t) = A_a(\rho)x_a(t) + B_a(\rho)W(t)u(t) + B_c y_c(t) + D_a(\rho)\xi(t)$$

where $B_c = [I_l \ \ 0]^T$ and

$$A_a(\rho) = \begin{bmatrix}0 & -C_p(\rho)\\ 0 & A_p(\rho)\end{bmatrix} B_a(\rho) = \begin{bmatrix}0\\ B(\rho)\end{bmatrix} D_a(\rho) = \begin{bmatrix}0\\ D_p(\rho)\end{bmatrix}.$$

Define the state transformation matrix (for the augmented system) according to $T_a = \mathrm{diag}(I_l, T_n)$. This induces regular form in the augmented system. In terms of the virtual control law a small change to v_l needs to be made to account for the reference signal:

$$v_l(t) = -S(\rho)(\tilde{A}(\rho)x(t) + \tilde{B}_c y_c(t)) - \dot{M}(\rho)x_1(t) + \Phi s(t) \tag{41}$$

where $\tilde{A}(\rho) = T_a A_a(\rho) T_a^{-1}$ and $\tilde{B}_c = T_a B_c$.

In the design which follows the LMIs are solved using YALMIP with the SEDUMI LMI solver.[4] In the LMIs, $A_a(\rho)$ has been replaced everywhere by $A_a(\rho) + \frac{1}{2}I_p$ to guarantee a level of exponential stability associated with the reduced order sliding motion, faster than $e^{-t/2}$. Such an axis shifting technique is standard. For implementation, a sigmoidal approximation of the discontinuous output injection signal from (29) has been used [18]

$$v_n = -\mathcal{K}(t,x)\frac{P_2 s(t)}{\|P_2 s(t)\| + \delta} \tag{42}$$

where δ is a small positive scalar.

The design freedom Φ from (28) was tuned to mitigate the degradation of tracking performance in the presence against wind/gust. Here, specifically, $\Phi = -0.5I_2$ was chosen. Then P_2 was calculated from solving an associated Lyapunov equation to yield $P_2 = I_2$. Since $B_2(\rho)$ and the range of ρ are known, the lower bound of $\|B_2(\rho)\|\|B_2^{\dagger}(\rho)\|$ from (32) can be found using the Matlab Symbolic toolbox. The value of $\Delta_{\max}$ is defined from equation (32) and can be determined once $\Delta(t)$, associated with the accuracy of estimation of the actuator health levels, is understood. From nonlinear simulations, the range of values of $\|v_l\|$ in (28) can be approximately determined. Furthermore the bound function $\alpha(t,x)$ in Assumption 2.2 can be estimated from wind/gust flight test data. Now only the values of $\mathcal{K}(\cdot)$ and δ from (42) are left to be selected. The final decision on the choice of these values was obtained via HIL testing. The control scheme was written in C-code using a template provided by JAXA to comply with the input-output interface of the FBW system. The controller was implemented on the FBW system using an explicit Euler solver based on a sample rate of 50Hz. Typical manoeuvres and pilot inputs were investigated in series of HIL tests to assess, via pilot feedback, the performance of the controller tuned on the nonlinear model. The HIL platform was used to tune $\mathcal{K}(\cdot)$ and δ in the unit vector term (42). Ideally, in any design $\mathcal{K}(\cdot)$ in (42) should be as small as possible, but large enough to provide robustness against matched uncertainty. Since in each channel $|v_{n,i}| \leq \mathcal{K}(\cdot)$, the allowed maximum magnitude of each control signal component gives an initial guess for an upper bound on the maximum allowed value $\mathcal{K}(\cdot)$. From this starting point, after some tuning and examining of the closed loop system performance for a range of faults, the values $\mathcal{K} = 0.4$ and $\delta = 0.05$ were settled on. This final design was then rigorously tested to ensure the control signals were chatter-free and were admissible in terms of the actuator range (again through HIL testing).

To simulate the presence of a fault estimation scheme and to model delays in decision making

$$\begin{aligned}\dot{\chi}(t) &= -0.5\chi(t) + 0.5W(t)\\ \Lambda(t) &= sat(\chi(t) + c)\end{aligned} \tag{43}$$

Consequently, when a fault is injected $\Lambda(t) \neq W(t)$. If $c = 0$ then $\Lambda(t) \to W(t)$ as $t \to \infty$ if $0 \leq W(t) \leq I$.

[3] Previous work in [24] has demonstrated that the lateral-directional motion can be captured sufficiently accurately using only v_{eas}.

[4] https://yalmip.github.io/solver/sedumi/

IV. Piloted Flight tests

In this section, results from the actual flight test campaign will be introduced and some flight test results will be used to demonstrate the efficacy of the scheme. These results represent the *first* sliding mode controller to be flight tested on the manned aircraft and represent a major milestone in the area of sliding mode FTC. The results presented here were obtained from flight campaigns supervised by a crew from JAXA, between 16-27 January 2017. The flight tests took place in Sagami Bay, south-west of Tokyo. During the test, the maximum recorded wind gust was 11.3m/s. Since the flight test campaign concentrated on the evaluation of lateral-directional control, longitudinal control of altitude and speed was manually maintained by the evaluation pilot using column and throttle lever inputs. In all flight tests, the v_{eas} was controlled around a value of 120 kts for different fixed altitudes in the range $600 - 1000m$. For the evaluation of the proposed lateral-directional controller, the commands were created manually by the evaluation pilot via wheel and pedal manipulations (which translate into roll and sideslip commands respectively). Detailed descriptions of each evaluation appear below:

Fault free: Two sets of fault-free flight test results are shown in Figs. 2-3. The manoeuvres were created by the evaluation pilot. In the first set (Fig. 2), a doublet manoeuvre ($\pm$20deg roll and $\pm$2deg sideslip angle) was created by the evaluation pilot; while in the second set (Fig. 3), a steady s-turn with a roll angle of $\pm 20deg$ is treated as the reference command. It is clear from Fig. 2(a) and Fig. 3(a) that sideslip and roll angle tracking performance are good. Figure 2(b) shows the corresponding sliding surfaces which demonstrate that sliding is maintained during the flight. The sliding corresponding to s-turn manoeuvre is also maintained, which is not shown here due to the length limit of the paper. The aileron and rudder commands and the actual surface deflections are shown in Fig. 2(c) and Fig. 3(b). From Fig. 2(c) and Fig. 3(b), it is clear the aileron and rudder are fault free.

Aileron faults only: In this subsection, test results when faults occur only on the aileron are shown in Fig. 4. It is assumed that the aileron works at 50% efficiency, that is, $K = \mathrm{diag}(1, 0.5, 0)$. The trajectories of the yaw and roll rates are shown in Fig. 4(a) wherein doublet commands are created by the evaluation pilot for both sideslip and roll angles. The yaw angle and side velocity are similar as those in Fig. 2(a). Clearly, although there exist aileron faults, the proposed scheme can still achieve good roll and sideslip tracking performance. Furthermore, during the flight tests, sliding is maintained and sliding surfaces are similar as those in Figure 2(b). The aileron and rudder commands and their surface deflections are also shown in Fig. 4(b). It can be seen that the aileron does not follow the commands due to the existence of faults.

Simultaneous aileron and rudder faults: Figure 5 illustrates the flight test results when faults occur on the aileron and the rudder simultaneously. Here the aileron and the rudder work at 50% efficiency and 80% efficiency respectively. In this case, $K = \mathrm{diag}(1, 0.5, 0.2)$. The trajectories of the lateral-directional states are shown in Fig. 5(a). Clearly, although

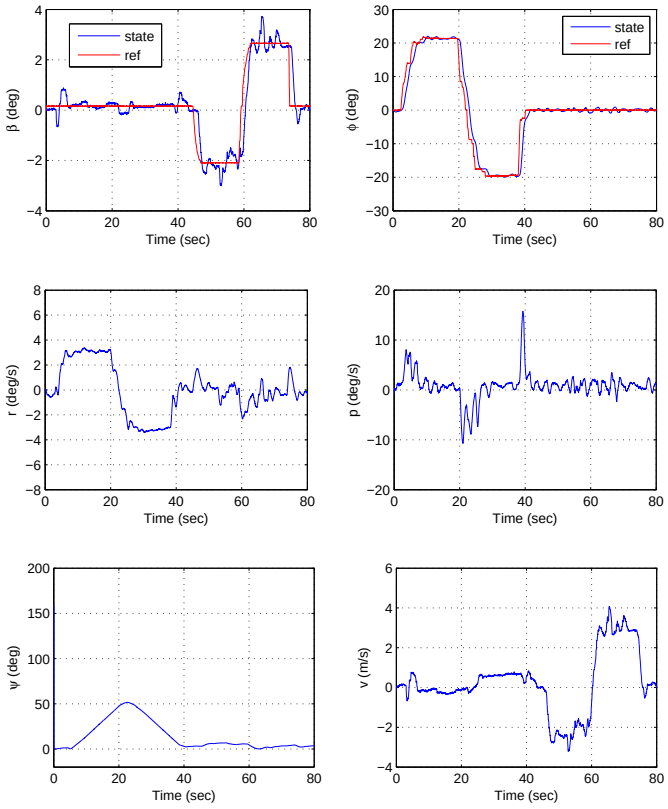

(a) The trajectories of the system states

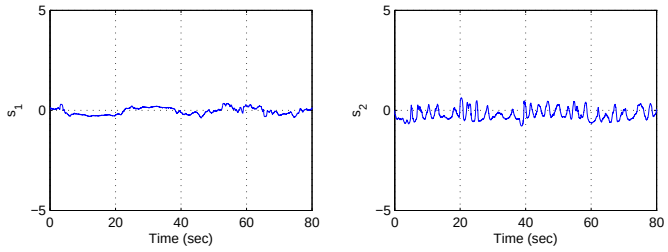

(b) Switching functions

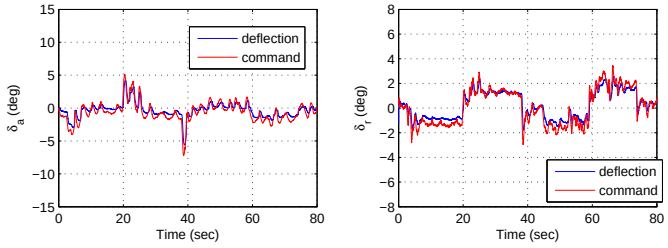

(c) Commands and surface deflections

Fig. 2. Fault-free case: states, switching functions and control surface deflections (Flight test)

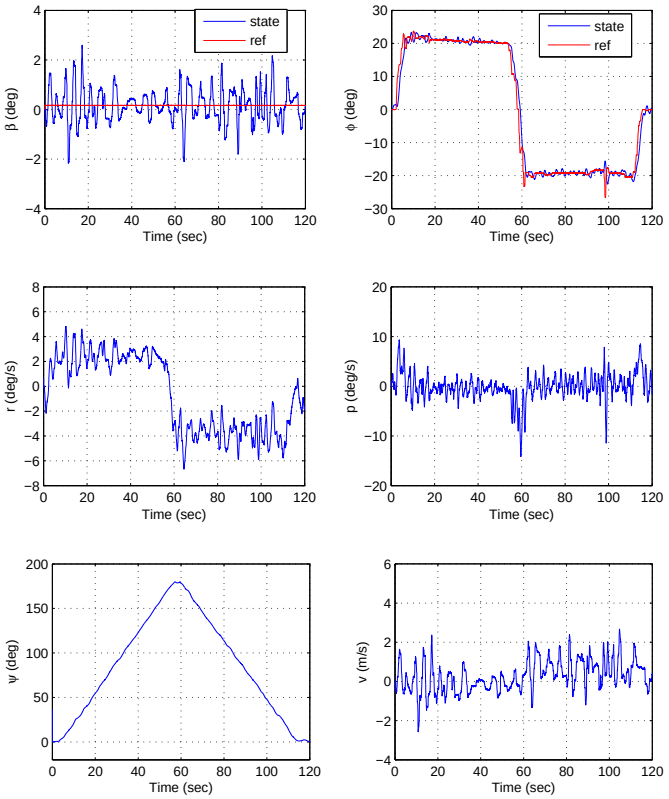

(a) The trajectories of the system states

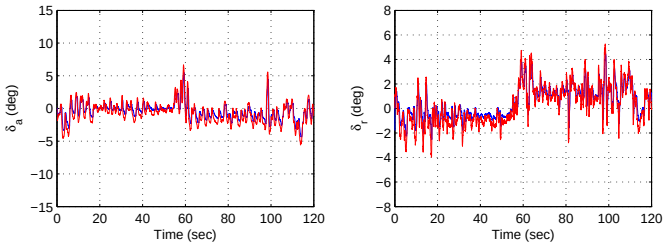

(b) Commands and surface deflections

Fig. 3. Fault-free case: states, switching functions and control surface deflections (Flight test for S-turn)

there exist simultaneous rudder and aileron faults, the proposed scheme can still achieve good roll and sideslip tracking performance. The aileron and rudder commands and their surface deflections are shown in Fig. 5(b). Clearly they cannot follow the respective commands due to the existence of faults.

V. Conclusion

This paper has developed an LPV sliding mode control allocation scheme in which online control allocation is used to utilize actuator availability in the face of actuator faults/failures, based on knowledge of the actuator efficiency (health) levels. The proposed scheme has been implemented on the JAXA's MuPAL-α research aircraft and validated during piloted flight tests. To the best of the authors' knowledge, these results represent the first published flight test of a sliding mode controller on a manned aircraft. The illustrated flight test results show that, during the manoeuvres induced by the

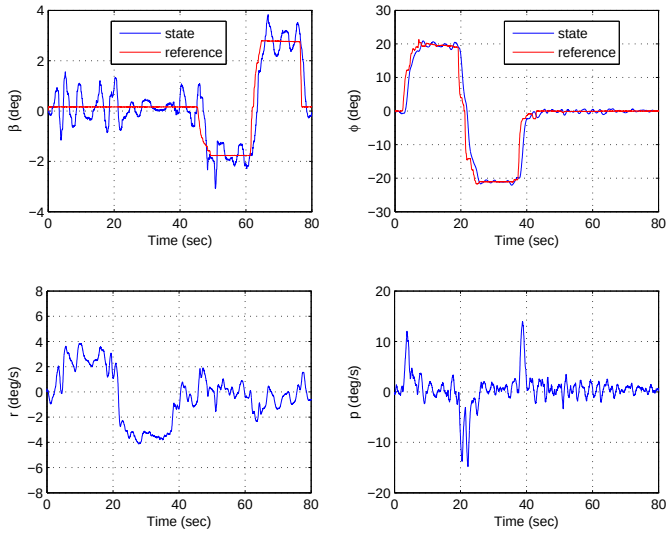

(a) The trajectories of the system states

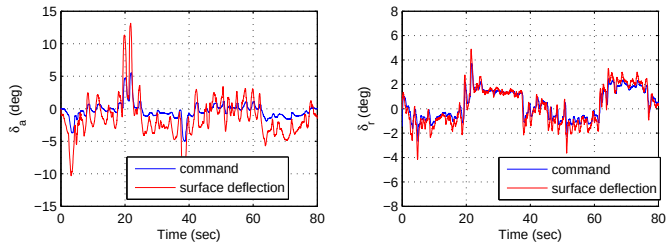

(b) Commands and surface deflections

Fig. 4. Aileron faults – $K = \mathrm{diag}(1, 0.5, 0)$: states, switching functions and control surface deflections (Flight test)

evaluation pilot, roll and sideslip tracking performance can be maintained in the face of rudder and aileron faults. In fact, during the flight tests, the evaluation pilot did not notice any change in behaviour of the aircraft when the actuator faults occurred.

Acknowledgement

This work was carried out while Dr Lejun Chen was at the University of Exeter funded by the European Union Horizon 2020 research and innovation programme under grant agreement No. 690811 and the Japan New Energy and Industrial Technology Development Organization under grant agreement No. 062800, as part of the EU/Japan joint research project entitled 'Validation of Integrated Safety-enhanced Intelligent flight cONtrol (VISION)'. We gratefully acknowledge the contributions of T. Hosoya, M. Naruoka, J. Kawaguchi, S. Morokuma, H. Ishii and Y. Sagara from JAXA and Y. Uetake from Nakanihon Air Service for their support in terms of the implementation and evaluations of the sliding mode control scheme on the MuPAL-α.

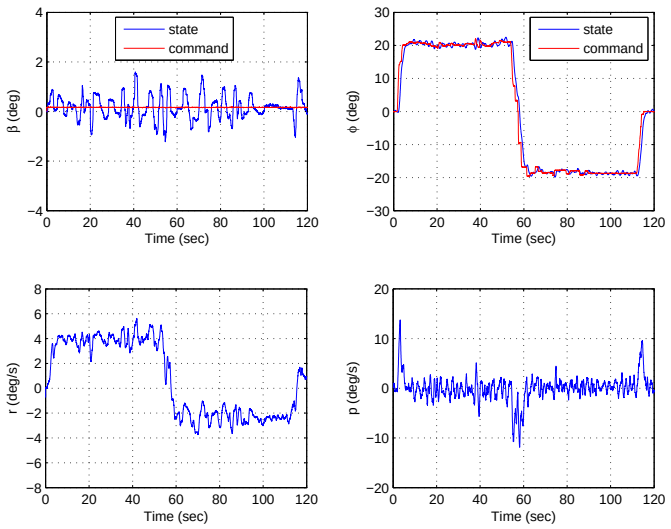

(a) The trajectories of the system states

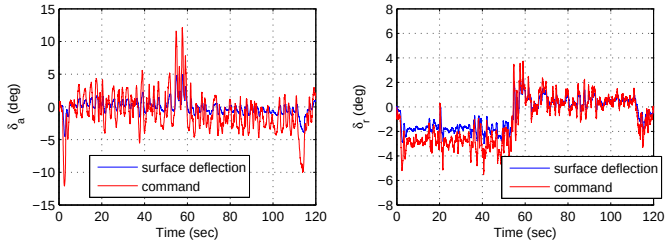

(b) Commands and surface deflections

Fig. 5. Aileron and rudder faults – $K = \mathrm{diag}(1, 0.5, 0.2)$: statesand control surface deflections (Flight test for S-turn)

REFERENCES

[1] M. Blanke, M. Kinnaert, J. Lunze, and M. Staroswiecki, *Introduction to Diagnosis and Fault-Tolerant Control*. Heidelberg: Springer Berlin Heidelberg, 2016.

[2] Y. Zhang and J. Jiang, "Bibliographical review on reconfigurable fault-tolerant control systems," *Annual Reviews in Control*, vol. 32, pp. 229–252, 2008.

[3] C. Edwards, T. Lombaerts, and H. Smaili, *Fault tolerant flight control: A benchmark challenge*. Springer, 2010.

[4] T. Lombaerts, E. Van Oort, Q.P. Chu, J. A. Mulder, and D. Joosten, "Online Aerodynamic Model Structure Selection and Parameter Estimation for Fault Tolerant Control," *J. Guid. Control Dyn*, vol. 33(3), pp. 707–723, 2010.

[5] H. Niemann and J. Stoustrup, "Integration of control and fault detection: Nominal and robust design," in *SAFEPROCESS '97*, pp. 331–336, 1997.

[6] J. M. Maciejowski and C. N. Jones, "MPC fault-tolerant flight control case study: flight 1862," *IFAC Proceedings Volumes*, vol. 36, pp. 119–124, 2003.

[7] S. Sivrioglu and K. Nonami, "Sliding Mode Control With Time-Varying Hyperplane for AMB Systems," *IEEE/ASME Transactions on Mechatronics*, vol. 3, pp. 51–59, 1998.

[8] P. Goupil, J. Boada-Bauxell, A. Marcos, P. Rosa, M. Kerr, and L. Dalbies, "An overview of the FP7 RECONFIGURE project: Industrial, scientific and technological objectives," in *SAFEPROCESS '15*, 2015.

[9] T. Tucker, *Touchdown: the development of propulsion controlled aircraft at NASA Dryden*, 1999.

[10] M. Sato and A. Satoh, "Flight control experiment of multipurpose-aviation-laboratory-α in-flight simulator," *Journal of Guidance, Control, and Dynamics*, vol. 34, 2011.

[11] J. Mohammadpour and C. Scherer, *Control of LPV Systems with Applications*. Springer, 2012.

[12] H. Alwi, C. Edwards, and C. P. Tan, *Fault Detection and Fault-Tolerant Control Using Sliding Modes*. Springer, 2011.

[13] A. Tapia, M. Bernal, and L. Fridman, "Nonlinear sliding mode control design: An LMI approach," *Systems & Control Letters*, vol.104, pp.38-44, 2017.

[14] H. D. Tuan, P. Apkarian, T. Narikiyo, and Y. Yamamoto, "Parameterized linear matrix inequality techniques in fuzzy control system design," *IEEE Trans Fuzzy Syst*, vol.9, pp.324-332, 2001.

[15] H. O. Wang, K. Tanaka, and M. F. Griffin, "An approach to fuzzy control of nonlinear systems: Stability and design issues," *IEEE Trans Fuzzy Syst*, vol.4, pp.14-23, 1996.

[16] H. Alwi and C. Edwards, "Fault tolerant control using sliding modes with on-line control allocation," *Automatica*, vol.44, pp.1859-66, 2008.

[17] O. Harkegard and S. Glad, "Resolving actuator redundancy - optimal vs. control allocation," *Automatica*, vol.41, pp.137–144, 2005.

[18] C. Edwards and S. K. Spurgeon, *Sliding Mode Control: Theory and Applications*. London. Taylor & Francis, 1998.

[19] D. Rotondo, F. Nejjari, V. Puig, and J. Blesa, "Model reference FTC for LPV systems using virtual actuator and set-membership fault estimation," *Int. J. Robust Nonlinear Control*, vol.25, pp.753-60, 2015.

[20] E. Feron, L. El Ghaoui, S.P. Boyd, and V.Balakrishnan, " *Linear Matrix Inequalities in System and Control Theory*", SIAM, 1994.

[21] L. Chen, H. Alwi, C. Edwards and M. Sato, "Hardware-in-the-loop evaluation of an LPV sliding mode fixed control allocation scheme on the MuPAL- research aircraft," *IEEE CCTA*, pp. 590-595, 2017.

[22] L. Chen, H. Alwi, C. Edwards and M. Sato, "Flight evaluation of an LPV sliding mode controller with online control allocation," *IEEE CDC*, pp. 3928-3933, 2017.

[23] H. Matsuki, T. Nishiyama, Y. Omori, S. Suzuki, K. Masui, M. Sato, "Flight test of fault-tolerant flight control system using simple adaptive control with PID controller," *Aircraft Eng and Aerospace Tech*, vol. 90, pp. 210-218, 2018.

[24] M. Sato, "Gain-Scheduled Flight Controller Using Bounded Inexact Scheduling Parameters," *IEEE Trans. Contr. Syst. Technol.*, vol. 26, pp. 1074-1082, 2018.

[25] M. Sato, "Robust model-following controller design for LTI systems affected by parametric uncertainties: a design example for aircraft motion", *International Journal of Control*, vol 82, pp. 689-704, 2009.

[26] B. Kolodziejczak and T. Szulc, "Convex combinations of matrices Full rank characterization", *Linear Algebra and its Applications*, vol. 287, pp.215-222, 1999.

[27] J. Bokor, G. Balas, "Detection filter design for LPV systems – a geometric approach", *Automatica*, vol. 40, pp. 511-518, 2004.